

UCSF

UC San Francisco Previously Published Works

Title

Mean Apparent Diffusion Coefficient Is a Sufficient Conventional Diffusion-weighted MRI Metric to Improve Breast MRI Diagnostic Performance: Results from the ECOG-ACRIN Cancer Research Group A6702 Diffusion Imaging Trial

Permalink

<https://escholarship.org/uc/item/48z7w4f1>

Journal

Radiology, 298(1)

ISSN

0033-8419

Authors

McDonald, Elizabeth S
Romanoff, Justin
Rahbar, Habib
[et al.](#)

Publication Date

2021

DOI

10.1148/radiol.2020202465

Peer reviewed

Mean Apparent Diffusion Coefficient Is a Sufficient Conventional Diffusion-weighted MRI Metric to Improve Breast MRI Diagnostic Performance: Results from the ECOG-ACRIN Cancer Research Group A6702 Diffusion Imaging Trial




Elizabeth S. McDonald, MD, PhD • Justin Romanoff, MA • Habib Rabbar, MD • Averi E. Kitsch, BS • Sara M. Harvey, MD • Jennifer G. Whisenant, PhD • Thomas E. Yankeelov, PhD • Linda Moy, MD • Wendy B. DeMartini, MD • Basak E. Dogan, MD • Wei T. Yang, MD • Lilian C. Wang, MD • Bonnie N. Joe, MD, PhD • Lisa J. Wilmes, PhD • Nola M. Hylton, PhD • Karen Y. Oh, MD • Luminita A. Tudorica, PhD • Colleen H. Neal, MD • Dariya I. Malyarenko, PhD • Christopher E. Comstock, MD • Mitchell D. Schnall, MD, PhD • Thomas L. Chenevert, PhD • Savannah C. Partridge, PhD

From the Department of Radiology, University of Pennsylvania Perelman School of Medicine, Philadelphia, Pa (E.S.M., M.D.S.); Center for Statistical Sciences, Brown University, Providence, RI (J.R.); Department of Radiology, University of Washington, 1144 Eastlake Ave E, LG2-200, Seattle, WA 98109 (H.R., A.E.K., S.C.P.); Departments of Radiology and Radiological Sciences (S.M.H.) and Medicine (J.G.W.), Vanderbilt University Medical Center, Nashville, Tenn; Vanderbilt-Ingram Cancer Center, Nashville, Tenn (J.G.W.); Department of Biomedical Engineering, University of Texas, Austin, Tex (T.E.Y.); Department of Radiology, New York University School of Medicine, New York, NY (L.M.); Department of Radiology, Stanford University School of Medicine, Stanford, Calif (W.B.D.); Department of Diagnostic Radiology, University of Texas Southwestern Medical Center, Dallas, Tex (B.E.D.); Department of Breast Imaging, MD Anderson Cancer Center, Houston, Tex (W.T.Y.); Department of Radiology, Northwestern University Feinberg School of Medicine, Chicago, Ill (L.C.W.); Department of Radiology and Biomedical Imaging, University of California, San Francisco School of Medicine, San Francisco, Calif (B.N.J., L.J.W., N.M.H.); Department of Radiology, Oregon Health and Science University, Portland, Ore (K.Y.O., L.A.T.); Department of Radiology/MRI, University of Michigan, Ann Arbor, Mich (C.H.N., D.I.M., T.L.C.); and Department of Radiology, Memorial Sloan-Kettering Cancer Center, New York, NY (C.E.C.). Received May 29, 2020; revision requested July 10; revision received September 11; accepted September 28. Address correspondence to S.C.P. (e-mail: scp3@uw.edu).

This study was coordinated by the Eastern Cooperative Oncology Group and American College of Radiology Imaging Network Cancer Research Group (Peter J. O'Dwyer, MD, and Mitchell D. Schnall, MD, PhD, group co-chairs) and supported by the National Cancer Institute of the National Institutes of Health under the following award numbers: U10CA180820, U10CA180794, U01CA079778, U01CA080098 (to the American College of Radiology Imaging Network), U01CA142565, U01CA166104, R01CA207290, R01CA203883, U01CA225427, UG1CA233328, UG1CA233270, UG1CA233320, UG1CA233160, UG1CA233329, UG1CA233302, and UG1CA233277. The study was also supported by the Cancer Prevention and Research Institute of Texas (CPRIT) RR160005 (T.E.Y. is a CPRIT scholar in cancer research).

The content is solely the responsibility of the authors and does not necessarily represent the official views of the National Institutes of Health. Mention herein of trade names, commercial products, or organizations does not imply endorsement by the U.S. government.

Conflicts of interest are listed at the end of this article.

Radiology 2021; 298:60–70 • <https://doi.org/10.1148/radiol.2020202465> • Content codes:   

Background: The Eastern Cooperative Oncology Group and American College of Radiology Imaging Network Cancer Research Group A6702 multicenter trial helped confirm the potential of diffusion-weighted MRI for improving differential diagnosis of suspicious breast abnormalities and reducing unnecessary biopsies. A prespecified secondary objective was to explore the relative value of different approaches for quantitative assessment of lesions at diffusion-weighted MRI.

Purpose: To determine whether alternate calculations of apparent diffusion coefficient (ADC) can help further improve diagnostic performance versus mean ADC values alone for analysis of suspicious breast lesions at MRI.

Materials and Methods: This prospective trial (ClinicalTrials.gov identifier: NCT02022579) enrolled consecutive women (from March 2014 to April 2015) with a Breast Imaging Reporting and Data System category of 3, 4, or 5 at breast MRI. All study participants underwent standardized diffusion-weighted MRI ($b = 0, 100, 600, \text{ and } 800 \text{ sec/mm}^2$). Centralized ADC measures were performed, including manually drawn whole-lesion and hotspot regions of interest, histogram metrics, normalized ADC, and variable b -value combinations. Diagnostic performance was estimated by using the area under the receiver operating characteristic curve (AUC). Reduction in biopsy rate (maintaining 100% sensitivity) was estimated according to thresholds for each ADC metric.

Results: Among 107 enrolled women, 81 lesions with outcomes (28 malignant and 53 benign) in 67 women (median age, 49 years; interquartile range, 41–60 years) were analyzed. Among ADC metrics tested, none improved diagnostic performance versus standard mean ADC (AUC, 0.59–0.79 vs AUC, 0.75; $P = .02$ –.84), and maximum ADC had worse performance (AUC, 0.52; $P < .001$). The 25th-percentile ADC metric provided the best performance (AUC, 0.79; 95% CI: 0.70, 0.88), and a threshold using median ADC provided the greatest reduction in biopsy rate of 23.9% (95% CI: 14.8, 32.9; 16 of 67 BI-RADS category 4 and 5 lesions). Nonzero minimum b value (100, 600, and 800 sec/mm^2) did not improve the AUC (0.74; $P = .28$), and several combinations of two b values (0 and 600, 100 and 600, 0 and 800, and 100 and 800 sec/mm^2 ; AUC, 0.73–0.76) provided results similar to those seen with calculations of four b values (AUC, 0.75; $P = .17$ –.87).

Conclusion: Mean apparent diffusion coefficient calculated with a two- b -value acquisition is a simple and sufficient diffusion-weighted MRI metric to augment diagnostic performance of breast MRI compared with more complex approaches to apparent diffusion coefficient measurement.

© RSNA, 2020

Online supplemental material is available for this article.

Abbreviations

ADC = apparent diffusion coefficient, AUC = area under the receiver operating characteristic curve, BI-RADS = Breast Imaging Reporting and Data System, ECOG-ACRIN = Eastern Cooperative Oncology Group and American College of Radiology Imaging Network, ROI = region of interest

Summary

An approach for measuring mean apparent diffusion coefficient that used two b values is sufficient for improving diagnostic performance of breast MRI and reducing the biopsy rate by up to 22.4% without lowering sensitivity.

Key Results

- No alternate metrics for apparent diffusion coefficient (ADC) improved diagnostic performance versus the commonly reported mean ADC (area under the receiver operating characteristic curve [AUC], 0.59–0.79 vs AUC, 0.75; $P = .02$ –.84), and maximum ADC had worse performance (AUC, 0.52; $P < .001$).
- The 25th-percentile ADC metric helped best distinguish malignant from benign abnormalities (AUC, 0.79), and median ADC provided the greatest biopsy rate reduction (23.9% [16 of 67 Breast Imaging Reporting and Data System category 4 and 5 lesions]).
- Using fewer b values (with maximum $b = 600$ – 800 sec/mm²) to calculate ADC did not affect diagnostic performance (AUC, 0.73–0.76; $P = .17$ –.87), which could simplify breast diffusion-weighted MRI acquisition and reduce imaging times.

Although it is clear that intravenous contrast material-enhanced breast MRI provides the highest sensitivity for detection of otherwise occult breast cancer, its main limitation as a supplemental screening tool is false-positive results that lead to unnecessary biopsies (1). Quantification of alterations in water diffusion through diffusion-weighted MRI holds strong potential to improve specificity of breast MRI by reflecting differences in lesion microstructure and cellularity (2,3). In vivo diffusion is most commonly reported as the apparent diffusion coefficient (ADC) metric, which numerous studies of breast diffusion-weighted MRI have shown to be useful in discriminating malignant from benign findings (4–10), as recently summarized in meta-analyses of 65 studies with more than 6400 pooled lesions (11).

Approaches for breast diffusion-weighted MRI in clinical research vary widely in acquisition and interpretation, and consensus recommendations from the European Society of Breast Radiology were recently published to facilitate standardization (12). However, diffusion-weighted MRI is not yet incorporated into the Breast Imaging Reporting and Data System (BI-RADS), and more data are needed to refine optimal methods for clinical implementation, particularly regarding quantitation of lesion ADC. Although ADC is commonly reported as the mean value across the lesion, measured using a manually defined region of interest (ROI) (2), studies suggest alternative metrics for ADC could further improve diagnostic performance. These alternative approaches include histogram-derived metrics (eg, minimum, maximum, and percentiles) to better account for cellular and microstructural heterogeneity within abnormalities (13); measuring the “hotspot” (subregion of greatest diffusion restriction and lowest ADC), potentially reflecting highest cellularity (14);

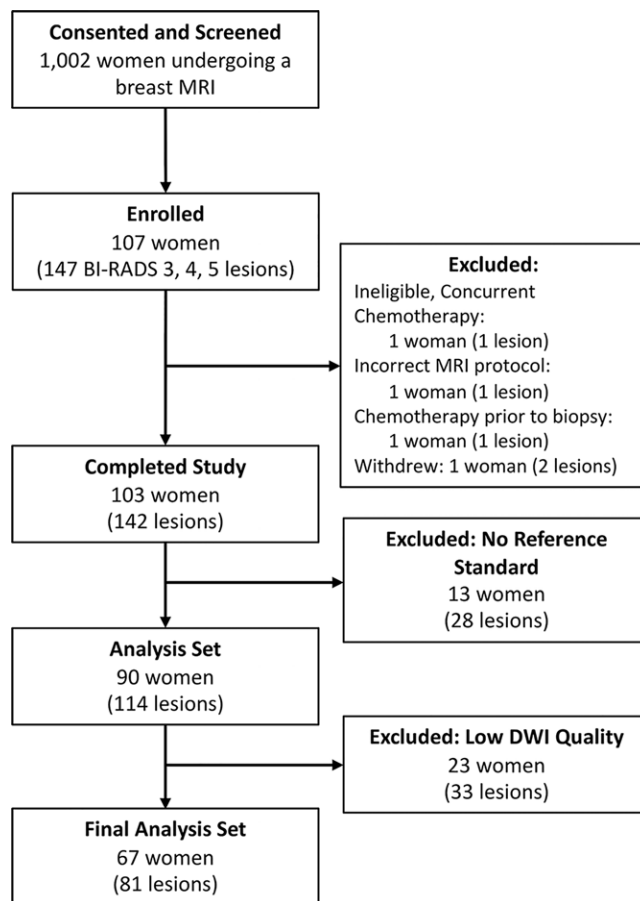


Figure 1: Eastern Cooperative Oncology Group and American College of Radiology Imaging Network Cancer Research Group A6702 trial participant flowchart. BI-RADS = Breast Imaging Reporting and Data System, DWI = diffusion-weighted imaging.

normalization of ADC to intrasubject fibroglandular tissue to account for variations in water content and hormonal influences (15); and using a nonzero minimum b value to reduce confounding perfusion effects in ADC calculation (10).

The Eastern Cooperative Oncology Group and American College of Radiology Imaging Network (ECOG-ACRIN) Cancer Research Group A6702 multicenter diffusion trial was designed to validate the performance of diffusion-weighted MRI for safely reducing false-positive findings at breast MRI by using a generalizable standardized approach. Results from the primary analysis of the trial identified a mean ADC threshold for a breast lesion (1.53×10^{-3} mm²/sec) to reduce biopsies by 21% without affecting sensitivity (16). As a prespecified secondary analysis of the trial, the purpose of our study was to test in the same cohort the hypothesis that alternative ADC metrics and/or b -value combinations can improve performance for diagnosing malignancy detected at dynamic contrast-enhanced MRI.

Materials and Methods

Study Participants

The ECOG-ACRIN A6702 trial was a single-arm, prospective, multi-institution imaging trial (ClinicalTrials.gov identifier:

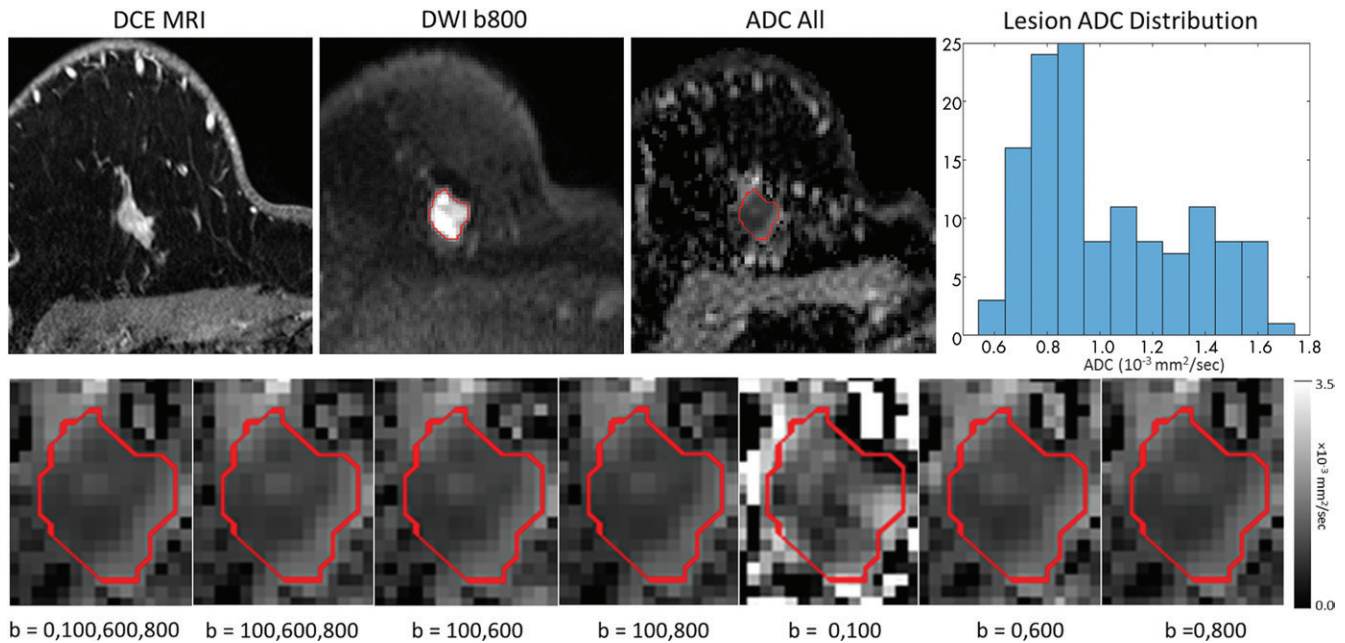


Figure 2: Malignant breast lesion in 41-year-old woman who underwent axial contrast material–enhanced MRI for evaluation of disease extent for new cancer diagnosis. Dynamic contrast-enhanced MRI demonstrated additional 19-mm irregular mass at 12 o'clock position in right breast, assessed as Breast Imaging Reporting and Data System category 5. At diffusion-weighted MRI, lesion mean apparent diffusion coefficient (ADC) was $1.10 \times 10^{-3} \text{ mm}^2/\text{sec}$, and ipsilateral normal tissue mean ADC was $1.43 \times 10^{-3} \text{ mm}^2/\text{sec}$. Representative T1-weighted postcontrast image (DCE), diffusion-weighted image (DWI) ($b = 800 \text{ sec}/\text{mm}^2$), ADC map created using all b values (0, 100, 600, and 800 sec/mm^2), and ADC histogram for lesion region of interest (shown in red on diffusion-weighted MRI scan and ADC images) are shown (top row, left to right). ADC maps were further generated for a variety of b -value combinations, as shown for lesion region (bottom row), including for nonzero minimum b values. Core-needle biopsy revealed invasive ductal carcinoma.

NCT02022579 [17,18]) performed at 10 academic institutions (Appendix E1 [online]) between March 2014 and April 2015. Each site received institutional review board approval and complied with the Health Insurance Portability and Accountability Act. In total, 1002 consecutive women aged 18 years or older undergoing breast MRI for any indication provided written informed consent to undergo a study-specific diffusion-weighted MRI sequence during their MRI examination. At clinical interpretation of non-diffusion-weighted MRI sequences (described below), 107 of 1002 women (11%) with at least one BI-RADS category 3, 4, or 5 lesion identified were enrolled (Fig 1) (16). Management of individual findings was based on the institutional standard of care, with the expectation that participants would undergo a biopsy after the study MRI (for BI-RADS category 4 or 5 lesions) or imaging follow-up at 6-month intervals for BI-RADS category 3 lesions.

Power analysis estimated that 85 evaluable lesions would provide 80% power for the primary analysis; thus, target enrollment was set for 100 participants to account for dropout (Appendix E1 [online]). The study sample was previously described in the primary analysis evaluating the diagnostic utility of mean ADC (16); this secondary analysis assessed the relative performance of various alternative ADC metrics. Data generated or analyzed during the study are available through ECOG-ACRIN.

MRI Protocol

The imaging protocol and quality assurance process for diffusion-weighted MRI have been previously reported (16). Diffusion-weighted MRI was performed at each site using a stan-

dardized protocol with a resolution of 1.5–2 mm in-plane and 4-mm section thickness. Before dynamic intravenous contrast-enhanced MRI, diffusion-weighted MRI was performed in the axial orientation with diffusion gradients in three orthogonal directions using multiple b values (0, 100, 600, and 800 sec/mm^2), with a single-shot, diffusion-weighted, spin-echo echo-planar imaging sequence with parallel imaging (reduction factor ≥ 2) and fat suppression. Scan parameters were repetition time, 4000 msec or greater; minimum echo time, 50–100 msec; flip angle, 90°; field of view, 30–36 cm; matrix, 180 \times 180 to 240 \times 240; and slice thickness, 4 mm without gap. Diffusion-weighted MRI acquisition time was approximately 5 minutes.

All sites were required to pass quality control testing consisting of diffusion-weighted MRI phantom imaging and submission of two in vivo diffusion-weighted MRI cases acquired by using the multi- b -value protocol (16). In vivo images were reviewed for absence of substantial artifacts, homogenous fat suppression, and adequate signal-to-noise ratio.

Interpretation of Clinical Breast MRI

MRI examinations for the 1002 women, who provided informed consent, were prospectively interpreted as part of routine clinical care by site radiologists (including H.R., S.M.H., L.M., W.B.D., B.E.D., W.T.Y., L.C.W., B.N.J., K.Y.O., C.H.N., and E.S.M.; reader experience summarized in Table E1 [online]) who used available clinical information but were initially blinded to diffusion-weighted MRI results, following study protocol. For each lesion identified, a final BI-RADS assessment was required based on only standard non-diffusion-

Table 1: Participant and Examination Features

Feature	Completed Study (<i>n</i> = 103)	Final Analysis Set (<i>n</i> = 67)
Median age at enrollment (y)*	47 (41–59) [24–75]	49 (41–60) [24–75]
Race		
Asian	7 (7)	4 (6)
Black or African American	6 (6)	5 (7)
Unknown	11 (11)	5 (7)
White	79 (77)	53 (79)
Ethnicity		
Hispanic or Latino	1 (1)	1 (1)
Not Hispanic or Latino	99 (96)	64 (96)
Unknown	3 (3)	2 (3)
Clinical indication for MRI		
Evaluation of extent of disease for known breast cancer	45 (44)	32 (48)
Further evaluation of lesion detected at other imaging	4 (4)	2 (3)
Short-interval follow-up MRI	6 (6)	4 (6)
Screening due to personal history of breast cancer	6 (6)	5 (7)
Screening due to genetic risk or family history of breast cancer	23 (22)	12 (18)
Other clinical indication	9 (9)	7 (10)
Multiple clinical indications	10 (10)	5 (7)
No. of BI-RADS category 3, 4, or 5 lesions		
1	75 (73)	57 (85)
2	19 (18)	6 (9)
3	7 (7)	4 (6)
4	2 (2)	0 (0)
Median maximum dimension of largest lesion at MRI (mm)*	11 (7–18) [4–110]	11 (8–20) [4–110]
MRI vendor		
GE (Waukesha, Wis)	19 (18)	14 (21)
Philips (Best, the Netherlands)	63 (61)	40 (60)
Siemens (Erlangen, Germany)	21 (20)	13 (19)
MRI field strength		
1.5 T	42 (41)	27 (40)
3.0 T	61 (59)	40 (60)

Note.—Except where indicated, data are numbers of patients, with percentages in parentheses. BI-RADS = Breast Imaging Reporting and Data System.

* Numbers in parentheses are interquartile ranges, and numbers in brackets are ranges.

weighted MRI sequences (19), and the following features were recorded: morphologic features (focus, mass, or non-mass enhancement), maximal size, kinetic enhancement worst curve type (initial phase: fast > medium > slow; delayed phase: washout > plateau > persistent), and signal intensity on T2-weighted images (low or high).

Centralized ADC Measurements

ADC values of eligible BI-RADS category 3, 4, and 5 breast lesions were measured by trained research scientists (including A.E.K., with 2 years of experience with breast diffusion-weighted MRI) at the University of Washington in consensus with the study cochairs (S.C.P. and H.R., with >15 and 7 years of experience with breast diffusion-weighted MRI, respectively), blinded to clinical outcomes, as described (16). Evaluability of diffusion-weighted MRI was first determined according to acceptable signal-to-noise ratio and fat suppression and absence of detrimental artifacts, distortions, and partial volume averaging.

Diffusion-weighted MR images were processed by using custom software originally developed in Matlab, version 2015a (MathWorks, Natick, Mass). ADC maps were calculated by using the standard monoexponential decay model (11) and linear least-squares fitting of the signal decay with increasing *b* value using all *b* values (0, 100, 600, and 800 sec/mm²), as in the primary analysis (16), and additionally for a variety of alternate two and three *b*-value combinations, including nonzero minimum *b* values.

For quantitation, each lesion was identified at diffusion-weighted MRI by cross-referencing with conventional intravenous contrast-enhanced and T2-weighted images to facilitate localization and to assist in avoiding adjacent fibroglandular or adipose tissue and regions of high T2 signal, such as a cyst or necrosis. A whole-lesion ROI was drawn on the *b* = 800 sec/mm² diffusion-weighted images, over multiple sections if necessary, with assistance of a semiautomated thresholding tool (20) to further exclude nonlesion voxels. ROIs were the same as those used in the primary analysis (not redrawn for this study). ROIs were then propagated to ADC maps (Fig 2).

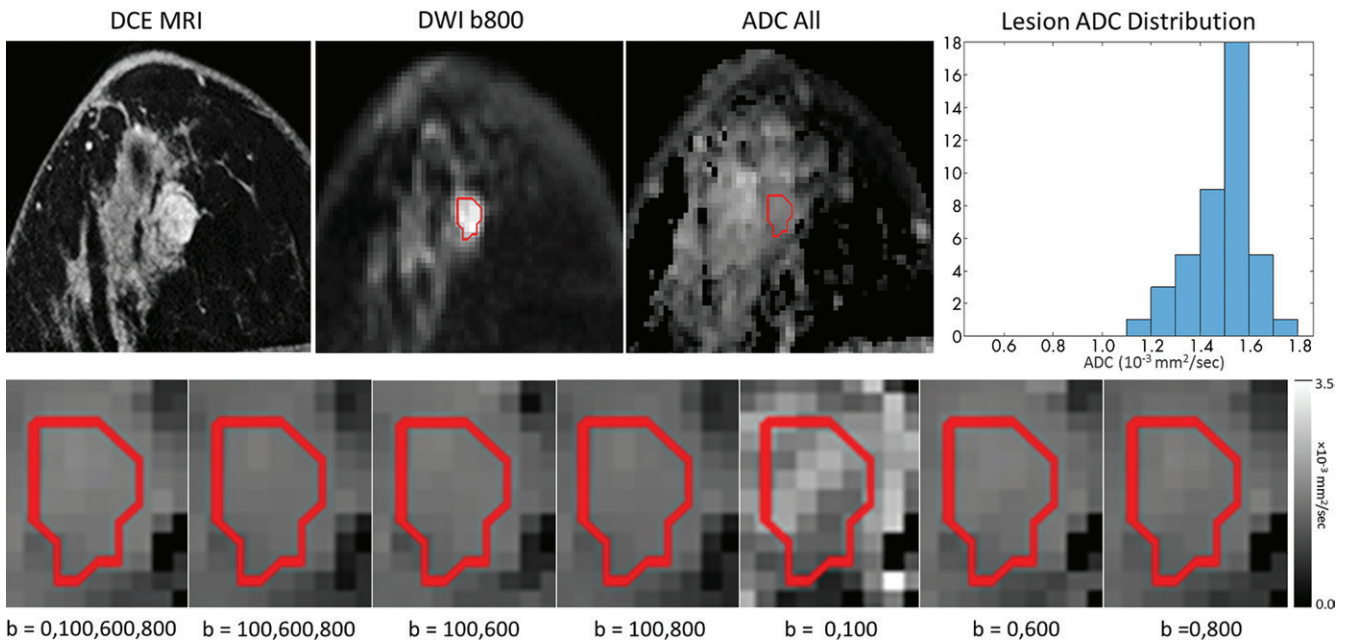


Figure 3: Benign breast lesion in 44-year-old woman who underwent axial contrast material-enhanced MRI for evaluation of disease extent for new cancer diagnosis. Dynamic contrast-enhanced MRI demonstrated additional 12-mm oval mass at 6 o'clock position in right breast, assessed as Breast Imaging Reporting and Data System category 4. At diffusion-weighted MRI, lesion mean apparent diffusion coefficient (ADC) was $1.49 \times 10^{-3} \text{ mm}^2/\text{sec}$, and ipsilateral normal tissue mean ADC was $1.44 \times 10^{-3} \text{ mm}^2/\text{sec}$. Representative T1-weighted postcontrast image (DCE), diffusion-weighted image (DWI) ($b = 800 \text{ sec}/\text{mm}^2$), ADC map created using all b values (0, 100, 600, and 800 sec/mm^2), and ADC histogram for lesion region of interest (shown in red on DWI scan and ADC images) are shown (top row, left to right). ADC maps were generated for a variety of b -value combinations, as shown for the lesion region (bottom row), including for nonzero minimum b values. Core-needle biopsy and excisional biopsy revealed benign atypical ductal hyperplasia.

For the all b -value fits (0, 100, 600, and 800 sec/mm^2), ADC was characterized through seven whole-lesion ROI histogram-based metrics (minimum, maximum, mean, median, 25th and 75th percentiles, and standard deviation). Hotspot ADC was also measured by averaging voxels for a small ROI (target size, 3×3 voxels) placed on the darkest part of the lesion on the ADC map (12). Normalized ADC was calculated as the ratio of the mean ADC in a lesion to that of normal tissue. A normal tissue ROI was drawn within the largest area of normal-appearing fibroglandular tissue (ipsilateral breast if possible) while minimizing inclusion of fat and areas with high T2 signal, such as cysts and fibroadenomas. Different b -value combinations were compared by using the whole-lesion mean ADC metric.

Reference Standard for Lesion Outcomes

The reference standard for each breast abnormality was determined with image-guided biopsy, surgery, or follow-up MRI at 12 months (as appropriate) (21,22) by institutional pathologists and radiologists blinded to centralized diffusion-weighted MRI measures (16). Briefly, the reference standard was considered indeterminate for BI-RADS category 4 or 5 lesions if no sampling was performed and if no follow-up MRI led to downgrading of the initial finding and also for lesions excised during surgery for another area (eg, an ipsilateral cancer) without previous sampling.

Statistical Analysis

In total, 14 alternative ADC metrics were analyzed for comparison with the standard mean ADC (using all b values)

reported for the primary analysis. Pearson correlation coefficients (r) were calculated between ADC metrics. Use of ADC metrics in discriminating malignant and benign abnormalities was evaluated by using receiver operating characteristic curve analysis. Each receiver operating characteristic curve was constructed empirically at the lesion level; the area under the receiver operating characteristic curve (AUC) was computed by using the trapezoidal rule, and its 95% CI was calculated by using 10 000 bootstrap replications and with normality assumed (23). For each metric, an optimal threshold to reduce biopsies was identified by maximizing specificity while maintaining 100% sensitivity. The reduction in biopsy rate was estimated as the number of BI-RADS category 4 and 5 lesions exceeding the ADC threshold, divided by the total number of BI-RADS category 4 and 5 lesions. Changes in biopsy rates were calculated as binomial proportions, and their 95% CIs were calculated using bootstrap percentiles.

As an additional analysis, two logistic regression models were fitted with generalized estimating equations and an exchangeable working correlation structure to estimate the performance of combining potentially complementary ADC metrics. The first model contained the mean ADCs calculated with b -value combinations of 0 and 100 sec/mm^2 and of 100, 600, and 800 sec/mm^2 , characterizing the faster (perfusion-weighted) and slower diffusion components, respectively. The second model combined the seven histogram-based metrics to account for intralesion heterogeneity. Each metric was centered and scaled to have zero mean and unit

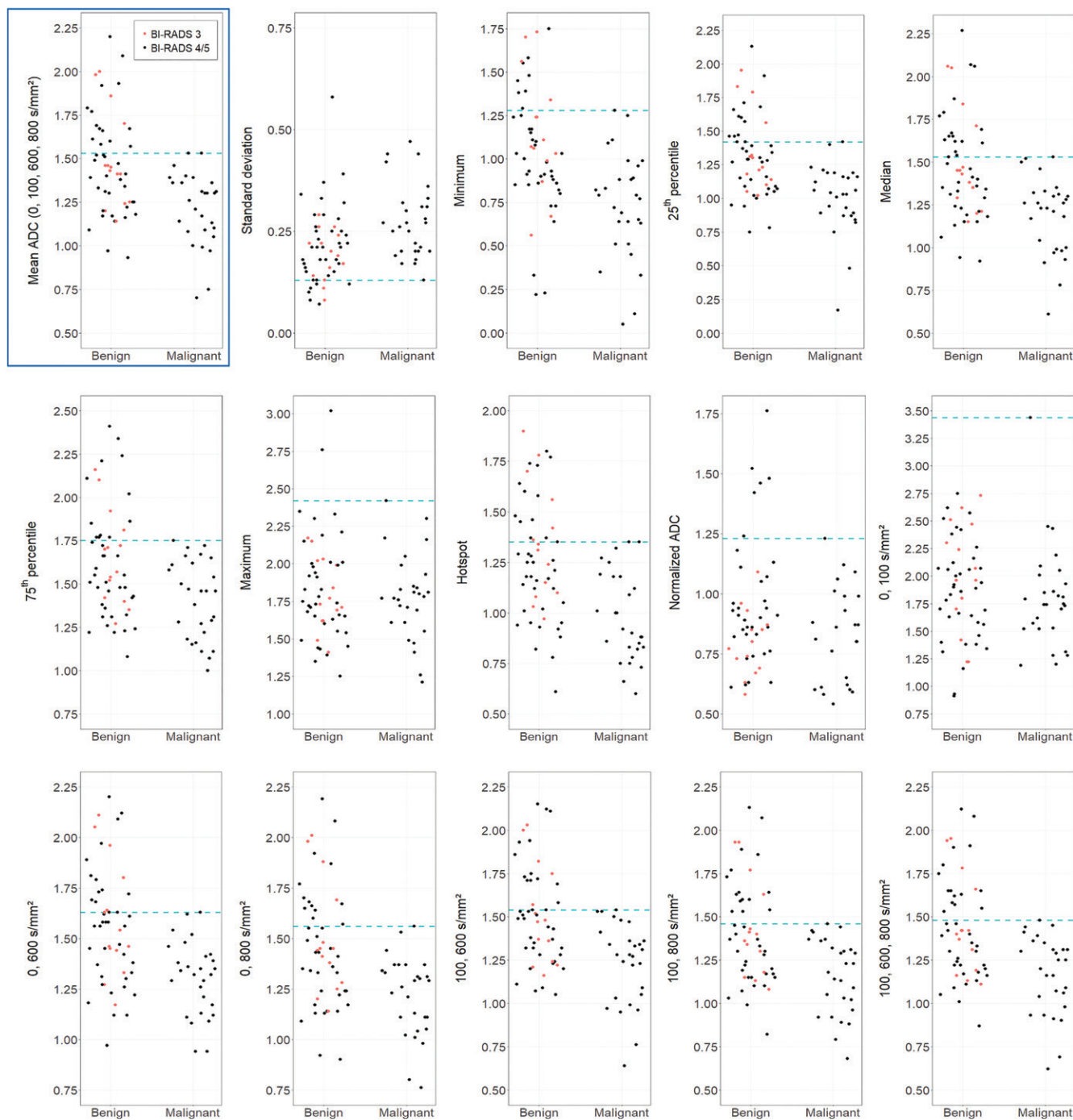


Figure 4: Scatterplots for apparent diffusion coefficient (ADC) metrics in malignant and benign lesions with associated thresholds. Standard mean ADC calculated from all b values, reported in Eastern Cooperative Oncology Group and American College of Radiology Imaging Network Cancer Research Group A6702 primary analysis, is shown in upper-left panel. All metrics were calculated in 81 evaluable lesions except normalized ADC, which was calculated for 73 lesions with measurable normal tissue. Measures for Breast Imaging Reporting and Data System (BI-RADS) category 4 and 5 lesions are shown in black, and measures for BI-RADS category 3 lesions are shown in red. Optimal threshold values (maintaining 100% sensitivity) for each metric are illustrated by blue dashed line. For all metrics except standard deviation, maximum malignant value was chosen as threshold value, where lesions above threshold could potentially avoid biopsy. For standard deviation with reverse association with malignancy, minimum malignant value was selected as threshold, and lesions with lower standard deviation could potentially avoid biopsy.

variance, and principal component analysis was performed on the transformed variables to remove multicollinearity. For each model, stratified fivefold cross-validation was used to estimate the AUC, and its 95% CI was calculated (24).

Two-sided P values were computed to test the hypothesis that the AUC of each alternative metric was different from the AUC

of the mean ADC calculated from all b values. The Bonferroni correction was used to account for the 14 comparisons made; $P < .0036$ ($.05/14$) was needed to reach a statistically significant difference. Analyses were performed with SAS/STAT software (version 9.4; SAS Institute, Cary, NC) and R software (version 4.0.2; the R Foundation for Statistical Computing, Vienna, Austria).

Table 2: Performance of Various ADC Metrics for Distinguishing Malignant and Benign Breast Lesions and Comparison with Previously Reported Mean ADC

Lesion ADC Metric	Benign Lesions (<i>n</i> = 53)	Malignant Lesions (<i>n</i> = 28)	AUC	<i>P</i> Value for Comparison to AUC of Mean ADC
Mean ADC (all <i>b</i> values: 0, 100, 600, 800 sec/mm ²)	1.47 ± 0.29	1.21 ± 0.21	0.75 (0.65, 0.84)	Reference
Alternative histogram metrics*				
Standard deviation	0.21 ± 0.09	0.27 ± 0.09	0.70 (0.59, 0.81)	.46
Minimum	1.05 ± 0.34	0.74 ± 0.30	0.76 (0.66, 0.87)	.84
25th percentile	1.32 ± 0.29	1.00 ± 0.26	0.79 (0.70, 0.88)	.06
Median	1.47 ± 0.30	1.19 ± 0.22	0.77 (0.67, 0.86)	.52
75th percentile	1.62 ± 0.31	1.41 ± 0.23	0.70 (0.59, 0.81)	.02
Maximum	1.83 ± 0.34	1.78 ± 0.28	0.52 (0.38, 0.65)	<.001
Hotspot ADC	1.26 ± 0.29	0.98 ± 0.22	0.78 (0.68, 0.88)	.50
Normalized ADC [†]	0.92 ± 0.26	0.83 ± 0.20	0.60 (0.43, 0.76)	.06
Alternative <i>b</i> values [‡]				
0, 100 sec/mm ²	1.90 ± 0.47	1.80 ± 0.46	0.59 (0.47, 0.72)	.02
0, 600 sec/mm ²	1.56 ± 0.28	1.30 ± 0.18	0.76 (0.67, 0.86)	.60
0, 800 sec/mm ²	1.46 ± 0.29	1.21 ± 0.20	0.75 (0.65, 0.85)	.69
100, 600 sec/mm ²	1.51 ± 0.29	1.23 ± 0.24	0.75 (0.65, 0.85)	.87
100, 800 sec/mm ²	1.41 ± 0.29	1.16 ± 0.22	0.73 (0.63, 0.83)	.17
100, 600, 800 sec/mm ²	1.43 ± 0.29	1.17 ± 0.23	0.74 (0.64, 0.84)	.28

Note.—Apparent diffusion coefficient (ADC) metrics are reported as $\times 10^{-3}$ mm²/sec (means \pm standard deviations). Numbers in parentheses are 95% CIs. *P* values are for testing the difference between the area under the receiver operating characteristic curve (AUC) of each alternative metric to the AUC of the mean ADC using all *b* values.

* Alternative histogram metrics were calculated by using all *b* values (0, 100, 600, and 800 sec/mm²).

[†] Normalized ADC was measurable for only 73 lesions (49 benign, 24 malignant) and were calculated by using all *b* values (0, 100, 600, and 800 sec/mm²).

[‡] The mean ADC metric was compared across alternative *b*-value combinations.

Results

Participant Characteristics

A total of 1002 women from 10 academic institutions provided informed consent before undergoing clinical MRI. Among these, 107 participants from nine institutions had at least one qualifying lesion and were enrolled (Fig 1). Forty women were excluded from the final analysis (one for concurrent chemotherapy, three for not completing the study, 13 for a missing reference standard, and 23 for a nonevaluable lesion at diffusion-weighted MRI); further details were previously reported (16). The final analysis comprised 67 women (median age, 49 years; interquartile range, 41–60 years; range, 24–75 years) with 81 lesions with a verified outcome reference standard (17 invasive carcinomas, 11 ductal carcinomas in situ, 53 benign lesions; median MRI size, 11 mm [interquartile range, 7–18 mm; range, 4–110 mm]) who underwent diffusion-weighted MRI at 1.5 T or 3.0 T for a variety of clinical indications (Table 1). Examples of ADC quantitation are shown for a malignant lesion (Fig 2) and a benign lesion (Fig 3). ADC measurements for malignant and benign abnormalities are shown for all metrics in Figure 4.

Alternate ROI Histogram Metrics

Of whole-tumor ADC histogram metrics, mean ADC was least correlated with standard deviation ADC ($r = -0.04$)

and most correlated with median ADC ($r = 0.99$ (Table E2 [online])). Higher standard deviation ADC was predictive of malignancy, suggesting increased intralesion heterogeneity, whereas for other histogram metrics, lower values were predictive of malignancy (Table 2; Fig 4). Compared with the diagnostic performance of mean ADC (AUC, 0.75; 95% CI: 0.65, 0.84), maximum ADC had a lower AUC (0.52; 95% CI: 0.38, 0.65; $P < .001$). The 25th-percentile ADC achieved the highest AUC among histogram metrics (0.79; 95% CI: 0.70, 0.88) but was not significantly different from mean ADC ($P = .06$) (Fig 5a; Table 2). AUCs of other histogram metrics were also not different (0.70–0.77; $P = .02$ –.84). For most metrics, a threshold corresponding to the maximum malignant value was selected to maintain sensitivity and to maximize specificity, where biopsy could potentially be avoided for lesions above the threshold. For standard deviation ADC, the minimum malignant value was selected as the threshold, and biopsy could be avoided for lesions below this value (Fig 4). Resulting reductions in the biopsy rate ranged widely across ADC histogram metrics, from 3.0% (two of 67 lesions) to 23.9% (16 of 67 lesions), with biopsy potentially avoided for 20.9% (14 of 67 lesions) of BI-RADS category 4 and 5 lesions on the basis of standard mean ADC (Fig 4; Table 3). Of note, the 25th-percentile metric, which achieved the highest AUC, yielded only a 16.4% (11 of 67 lesions) reduction in biopsies.

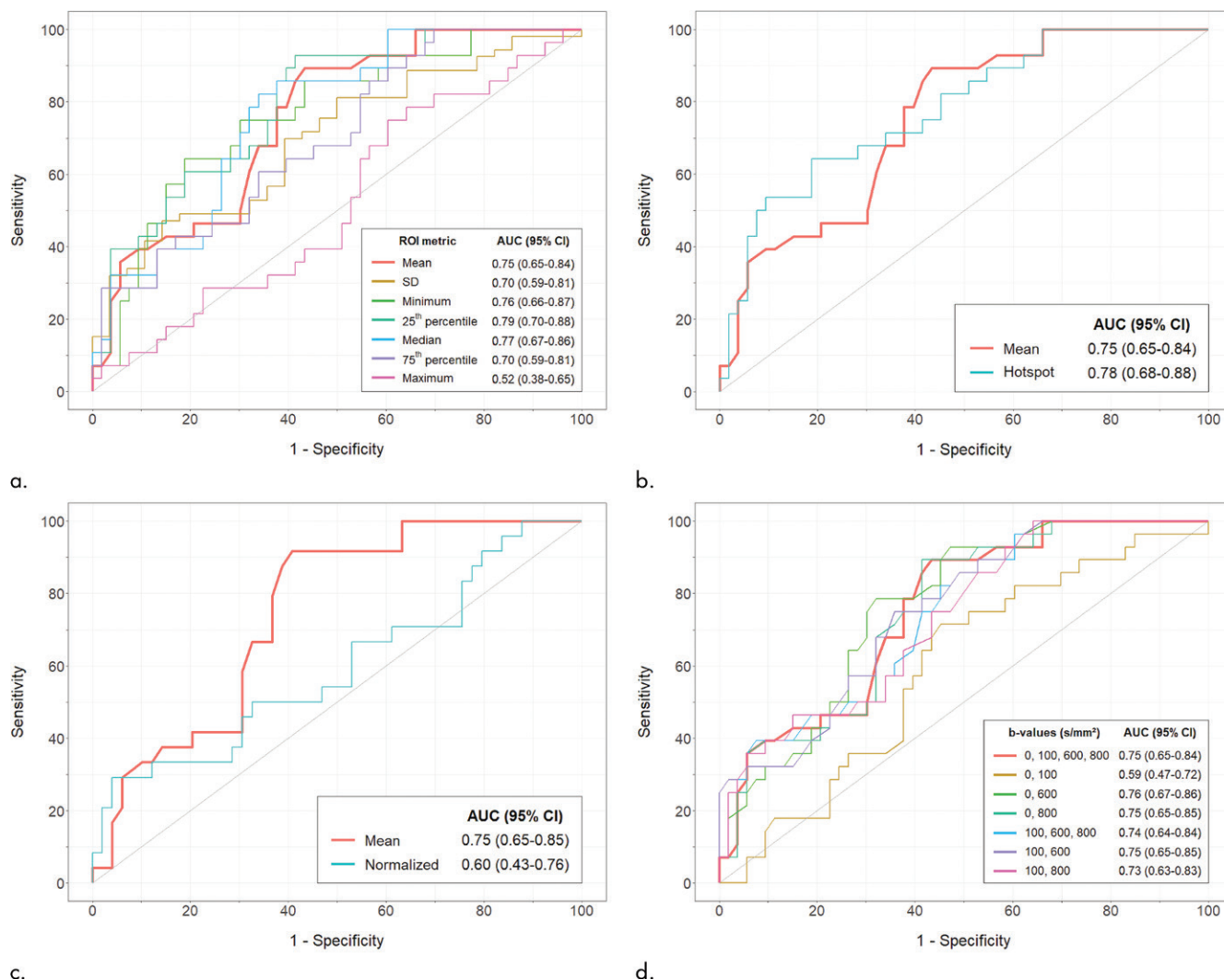


Figure 5: Receiver operating characteristic curves for all apparent diffusion coefficient (ADC) metrics. **(a)** Graph shows histogram-based ADC metrics from whole-lesion regions of interest (ROI) ($n = 81$ lesions). **(b)** Graph shows hotspot ADC ($n = 81$ lesions). **(c)** Graph shows normalized ADC ($n = 73$ lesions, normal tissue was not measurable in eight women). **(d)** Graph shows mean ADCs calculated with varying b -value combinations ($n = 81$ lesions). Reference mean ADC calculated using all b values (0, 100, 600, and 800 sec/mm^2) is shown on each plot for comparison (red line). AUC = area under the receiver operating characteristic curve, SD = standard deviation.

Hotspot ADC

Hotspot ADC was strongly correlated with whole-tumor mean ADC ($r = 0.88$) (Table E2 [online]). Hotspot ADC achieved an AUC of 0.78 (95% CI: 0.68, 0.88), which was not different from whole-tumor mean ADC ($P = .50$) (Fig 5b; Table 2) but demonstrated a slightly lower biopsy reduction rate of 17.9% (12 of 67 lesions) (Table 3).

Normalized ADC

Normalized ADC could not be calculated for eight lesions in eight women (seven without sufficient normal-appearing fibroglandular tissue, one with image artifact affecting normal tissue regions); the subset for normalized ROI ADC comparisons was 73 lesions in 59 women. Normal tissue was sampled in the ipsilateral breast for 70 lesions and in the contralateral breast for three lesions with no normal-appearing ipsilateral breast tissue. Standard mean ADC and normalized ADC measures were only moderately correlated ($r = 0.63$) (Table E2 [online]). Normalized ADC yielded an AUC of 0.60 (95% CI: 0.43,

0.76) for differentiating malignant from benign lesions, which did not improve performance over standard ADC (AUC, 0.75; 95% CI: 0.65, 0.85; $P = .06$) (Fig 5c; Table 2). The biopsy reduction rate of 10.2% (six of 59 BI-RADS category 4 and 5 lesions) according to normalized ADC threshold was also not an improvement versus standard ADC (Table 3).

Alternate b-Value Combinations

Mean ADC measures calculated with different b -value combinations were highly correlated ($r \geq 0.94$), with the exception of the low b -value combination of 0 and 100 sec/mm^2 ($r = 0.20$ –0.45) (Table E3 [online]). Compared with the reference using all b values (0, 100, 600, and 800 sec/mm^2) with an AUC of 0.75 (95% CI: 0.65, 0.84), there was no difference in AUC for any tested combination of b values (AUC, 0.59–0.76; $P = .02$ –.87), including ADC calculated with a nonzero b -value minimum (b values of 100, 600, and 800 sec/mm^2 ; AUC, 0.74; 95% CI: 0.64, 0.84). Of note, several combinations of two b values (ie, 0 and 600, 100

Table 3: Estimated Reduction in Biopsy Rate of BI-RADS Category 4 and 5 Lesions While Maintaining Sensitivity for Various Apparent Diffusion Coefficient Metrics

Lesion ADC Metric	ADC Threshold with 100% Sensitivity ($\times 10^{-3}$ mm ² /sec)	Reduction in Biopsy Rate Using ADC Threshold*
Mean ADC (0, 100, 600, 800 sec/mm ²)	1.53	14/67 (20.9) [11.2, 31.2]
Alternative histogram metrics		
Standard deviation	0.13	6/67 (9.0) [2.9, 15.9]
Minimum	1.28	8/67 (11.9) [4.7, 19.7]
25th percentile	1.42	11/67 (16.4) [8.3, 25.0]
Median	1.53	16/67 (23.9) [14.8, 32.9]
75th percentile	1.75	12/67 (17.9) [9.7, 26.6]
Maximum	2.42	2/67 (3.0) [0.0, 7.7]
Hotspot ADC	1.35	12/67 (17.9) [9.7, 26.7]
Normalized ADC [†]	1.23	6/59 (10.2) [3.4, 18.0]
Alternative <i>b</i> values		
0, 100 sec/mm ²	3.44	0/67 (0.0)
0, 600 sec/mm ²	1.63	12/67 (17.9) [9.5, 26.9]
0, 800 sec/mm ²	1.56	13/67 (19.4) [10.8, 28.4]
100, 600 sec/mm ²	1.54	13/67 (19.4) [11.1, 28.1]
100, 800 sec/mm ²	1.46	15/67 (22.4) [13.6, 31.3]
100, 600, 800 sec/mm ²	1.48	15/67 (22.4) [13.6, 31.3]

* Reductions in biopsy rate are expressed as fractions, with percentages in parentheses and 95% CIs in brackets. Threshold was applied in all Breast Imaging Reporting and Data System (BI-RADS) category 4 and 5 lesions ($n = 67$ total, 28 malignant, 39 benign).

[†] Normalized ADC was not measurable for eight BI-RADS category 4 and 5 lesions in eight women.

and 600, 0 and 800, and 100 and 800 sec/mm²) provided performance similar to that of the reference combination of four *b* values, and the choice of maximum *b* value (600 vs 800 sec/mm²) did not affect diagnostic performance (Fig 5d; Table 2). Aside from a *b*-value combination of 0 and 100 sec/mm², with a 0% biopsy rate reduction, biopsy rate reductions according to ADC thresholds ranged closely from 17.9% (12 of 67 lesions) to 22.4% (15 of 67 lesions) across various *b*-value combinations (Table 3).

Exploratory Multivariable Performance

Two exploratory models were evaluated: model 1 combining mean ADCs using complementary *b*-value combinations (0 and 100 sec/mm² and 100, 600, and 800 sec/mm²; $r = 0.23$) (Table E3 [online]), and model 2 combining whole-tumor histogram-based metrics. For model 2, principal component analysis was applied to the transformed histogram metrics; the first two principal components explained 95% of the total variance and were entered into the model. Compared with the mean ADC (AUC, 0.75; 95% CI: 0.64, 0.85), model 2 suggested improved performance for predicting malignancy (AUC, 0.80; 95% CI: 0.71, 0.88), whereas model 1 did not (AUC, 0.67; 95% CI: 0.57, 0.78).

Discussion

As breast MRI use grows to include screening women of intermediate risk (25,26), strong interest exists in finding ways to mitigate the primary risk of this tool: increased false-positive results and unnecessary biopsies. Many benign pathologic abnormalities and even normal parenchymal tissues exhibit

suspicious enhancement at dynamic contrast material-enhanced MRI, resulting in a cancer diagnosis for only one in five screening MRI-prompted biopsies (21) and limiting the cost-effectiveness of this highly sensitive tool (27). Evidence from multiple studies demonstrates the potential of diffusion-weighted MRI to improve the diagnostic performance of dynamic contrast-enhanced MRI, but standardization and optimization of the approach are needed for widespread clinical implementation (28).

Using data from the ECOG-ACRIN A6702 multicenter trial, we evaluated a variety of lesion ADC metrics accounting for intralesion heterogeneity and interparticipant variability and probing different underlying biologic properties. These metrics demonstrated AUCs ranging from 0.52 to 0.79 for diagnosing malignancy, and even the highest-performing metrics (AUC >0.75) did not significantly improve on the benchmark established from the primary analysis of the trial using mean ADC (AUC, 0.75; $P = .06-.84$). The 25th-percentile and hotspot ADC metrics, both potentially sampling the most viable cellular regions, achieved the highest AUCs (0.79 and 0.78, respectively), but neither improved on mean ADC performance for reducing unnecessary biopsies. Use of fewer than four *b* values, with a maximum *b* value of 600 or 800 m/sec², did not affect performance (AUCs, 0.73–0.76; $P = .17-.87$). Our results therefore suggest that mean ADC alone, potentially with use of only two *b* values, is sufficient to improve specificity of conventional contrast-enhanced breast MRI and to reduce unnecessary biopsies.

Many studies have explored ADC for differentiation of suspicious breast findings (28–30). The primary analysis from our multicenter prospective trial extends this work to provide a generalizable ADC threshold to reduce unnecessary biopsies in

current clinical practice, less prone to potential biases of single-institution retrospective studies. This secondary analysis demonstrates the robustness of ADC as a diagnostic marker in breast abnormalities because (with few exceptions) variable measurement approaches did not notably affect diagnostic performance. Whole-tumor or hotspot ROI approaches yielded similar diagnostic performance, although differences in their ADC threshold values (1.53 and 1.35×10^{-3} mm²/sec, respectively) must be considered during interpretations. Similarly, optimal ADC thresholds varied with *b*-value combinations and were higher with use of minimum *b* values of 0 versus 100 sec/mm² and/or maximum *b* values of 600 versus 800 sec/mm². Our findings build on previous studies investigating optimal *b*-value combinations (10,11,31,32) and support using the two-*b*-value combination of 0 and 800 sec/mm² as proposed in recent consensus recommendations (12), allowing for minimization of diffusion-weighted MRI examination time and improved suitability for abbreviated breast MRI protocols.

Our study had several limitations. The trial was not powered for secondary analyses, and larger sample sizes may be needed to identify subtle differences in diagnostic performance. In addition, the Bonferroni correction was selected as a conservative approach (because not all comparisons were prespecified), which may limit sensitivity to detect differences. Moreover, we explored only monoexponential ADC modeling over a limited *b*-value range, whereas more advanced diffusion-weighted MRI modeling may better characterize tissue microstructure and improve performance (33–35).

In conclusion, our multicenter trial provided evidence supporting the use of standard mean ADC using acquisition with two *b* values (eg, 0 and 800 sec/mm²) as a simple and sufficient diffusion-weighted MRI metric to augment dynamic contrast-enhanced MRI diagnostic performance, rather than more complex alternative metrics, which may be more time-consuming to obtain. Still, exploratory multivariable analysis suggested opportunities to further improve performance of diffusion-weighted MRI (eg, through combined histogram metrics), warranting investigation in larger studies. An important next step toward clinical standardization is to validate the performance of diffusion-weighted MRI using the data and optimal cutoffs learned from this trial in larger retrospective data sets and/or prospective trials.

Acknowledgments: The authors thank the women who participated in this trial and the Eastern Cooperative Oncology Group and American College of Radiology Imaging Network 6702 investigators and research staff at all participating sites. We also thank Debosmita Biswas, MS, for additional assistance with image analysis and figures.

Author contributions: Guarantors of integrity of entire study, E.S.M., L.M., D.I.M., S.C.P.; study concepts/study design or data acquisition or data analysis/interpretation, all authors; manuscript drafting or manuscript revision for important intellectual content, all authors; approval of final version of submitted manuscript, all authors; agrees to ensure any questions related to the work are appropriately resolved, all authors; literature research, E.S.M., H.R., T.E.Y., L.M., B.N.J., D.I.M., C.E.C., S.C.P.; clinical studies, E.S.M., H.R., J.G.W., T.E.Y., W.B.D., B.E.D., B.N.J., L.J.W., K.Y.O., L.A.T., C.H.N., S.C.P.; experimental studies, E.S.M., A.E.K., B.N.J., L.J.W., N.M.H., L.A.T., C.H.N., M.D.S., T.L.C., S.C.P.; statistical analysis, J.R., D.I.M., S.C.P.; and manuscript editing, E.S.M., J.R., H.R., S.M.H., T.E.Y., L.M., W.B.D., B.E.D., W.T.Y., L.C.W., B.N.J., L.J.W., N.M.H., K.Y.O., L.A.T., C.H.N., D.I.M., C.E.C., M.D.S., T.L.C., S.C.P.

Disclosures of Conflicts of Interest: E.S.M. disclosed no relevant relationships. J.R. Activities related to the present article: institution received grant from National Cancer Institute. Activities not related to the present article: disclosed no relevant relationships. Other relationships: disclosed no relevant relationships. H.R. Activities related to the present article: institution received grant from National Cancer Institute. Activities not related to the present article: is an uncompensated consultant for Philips Healthcare; has grants/grants pending with GE Healthcare. Other relationships: disclosed no relevant relationships. A.E.K. disclosed no relevant relationships. S.M.H. disclosed no relevant relationships. J.G.W. Activities related to the present article: institution received grant from National Cancer Institute. Activities not related to the present article: receives royalties from Anasys Instruments. Other relationships: disclosed no relevant relationships. T.E.Y. Activities related to the present article: institution received grant from National Cancer Institute. Activities not related to the present article: disclosed no relevant relationships. Other relationships: disclosed no relevant relationships. L.M. Activities related to the present article: disclosed no relevant relationships. Activities not related to the present article: receives payment from iCAD for board membership; institution has grants/grants pending with Siemens; holds stock/stock options in Lunit. Other relationships: disclosed no relevant relationships. W.B.D. Activities related to the present article: institution received grant from Eastern Cooperative Oncology Group and American College of Radiology Imaging Network. Activities not related to the present article: disclosed no relevant relationships. Other relationships: disclosed no relevant relationships. B.E.D. Activities related to the present article: institution received grant from National Cancer Institute. Activities not related to the present article: is a consultant for Endomag. Other relationships: disclosed no relevant relationships. W.T.Y. Activities related to the present article: disclosed no relevant relationships. Activities not related to the present article: serves on the board of Braid Health; is a consultant for Seno Medical; receives book royalties from Elsevier; receives payment from GE Healthcare for Scientific Advisory Board membership; is a Scientific Advisory Board member for Siemens Medical. Other relationships: disclosed no relevant relationships. L.C.W. disclosed no relevant relationships. B.N.J. disclosed no relevant relationships. L.J.W. disclosed no relevant relationships. N.M.H. Activities related to the present article: institution received grant from Eastern Cooperative Oncology Group and American College of Radiology Imaging Network. Activities not related to the present article: disclosed no relevant relationships. Other relationships: disclosed no relevant relationships. K.Y.O. Activities related to the present article: disclosed no relevant relationships. Activities not related to the present article: institution received U01 grant; received payment for lectures, including service on speakers bureaus; receives royalties from Elsevier. Other relationships: disclosed no relevant relationships. L.A.T. disclosed no relevant relationships. C.H.N. disclosed no relevant relationships. D.I.M. disclosed no relevant relationships. C.E.C. disclosed no relevant relationships. M.D.S. Activities related to the present article: institution received grant from National Institutes of Health. Activities not related to the present article: institution has grants/grants pending with Siemens Healthineers. Other relationships: disclosed no relevant relationships. T.L.C. Activities related to the present article: disclosed no relevant relationships. Activities not related to the present article: disclosed no relevant relationships. Other relationships: is co-inventor of IP assigned to and managed by the University of Michigan (by research agreement, Philips has nonexclusive royalty-free use of this IP; the IP was not used in this study); is co-inventor of IP assigned to and managed by the University of Michigan (ImBio paid license fees to use this IP; the IP is only peripherally related to topic of this work, and ImBio was not a part of this study. ImBio products were not used for this study.) S.C.P. Activities related to the present article: institution received grants from National Institutes of Health and National Cancer Institute. Activities not related to the present article: institution has grants/grants pending with GE Healthcare; institution received in-kind research support from Philips Healthcare. Other relationships: disclosed no relevant relationships.

References

- Melnikow J, Fenton JJ, Whitlock EP, et al. Supplemental screening for breast cancer in women with dense breasts: a systematic review for the U.S. preventive services task force. *Ann Intern Med* 2016;164(4):268–278.
- Partridge SC, McDonald ES. Diffusion weighted magnetic resonance imaging of the breast: protocol optimization, interpretation, and clinical applications. *Magn Reson Imaging Clin N Am* 2013;21(3):601–624.
- Mann RM, Cho N, Moy L. Breast MRI: state of the art. *Radiology* 2019;292(3):520–536.
- Partridge SC, DeMartini WB, Kurland BF, Eby PR, White SW, Lehman CD. Quantitative diffusion-weighted imaging as an adjunct to conventional breast MRI for improved positive predictive value. *AJR Am J Roentgenol* 2009;193(6):1716–1722.
- Woodhams R, Matsunaga K, Kan S, et al. ADC mapping of benign and malignant breast tumors. *Magn Reson Med Sci* 2005;4(1):35–42.
- Park MJ, Cha ES, Kang BJ, Ihn YK, Baik JH. The role of diffusion-weighted imaging and the apparent diffusion coefficient (ADC) values for breast tumors. *Korean J Radiol* 2007;8(5):390–396.
- Marini C, Iacconi C, Giannelli M, Cilotti A, Moretti M, Bartolozzi C. Quantitative diffusion-weighted MR imaging in the differential diagnosis of breast lesion. *Eur Radiol* 2007;17(10):2646–2655.

8. Baltzer PA, Renz DM, Herrmann KH, et al. Diffusion-weighted imaging (DWI) in MR mammography (MRM): clinical comparison of echo planar imaging (EPI) and half-Fourier single-shot turbo spin echo (HASTE) diffusion techniques. *Eur Radiol* 2009;19(7):1612–1620.
9. Guo Y, Cai YQ, Cai ZL, et al. Differentiation of clinically benign and malignant breast lesions using diffusion-weighted imaging. *J Magn Reson Imaging* 2002;16(2):172–178.
10. Bogner W, Gruber S, Pinker K, et al. Diffusion-weighted MR for differentiation of breast lesions at 3.0 T: how does selection of diffusion protocols affect diagnosis? *Radiology* 2009;253(2):341–351.
11. Baxter GC, Graves MJ, Gilbert FJ, Patterson AJ. A meta-analysis of the diagnostic performance of diffusion MRI for breast lesion characterization. *Radiology* 2019;291(3):632–641.
12. Baltzer P, Mann RM, Lima M, et al. Diffusion-weighted imaging of the breast—a consensus and mission statement from the EUSOBI International Breast Diffusion-Weighted Imaging working group. *Eur Radiol* 2020;30(3):1436–1450.
13. Li X, Kang H, Arlinghaus LR, et al. Analyzing spatial heterogeneity in DCE- and DW-MRI parametric maps to optimize prediction of pathologic response to neoadjuvant chemotherapy in breast cancer. *Transl Oncol* 2014;7(1):14–22.
14. Arponen O, Sudah M, Masarwah A, et al. Diffusion-weighted imaging in 3.0 Tesla breast MRI: diagnostic performance and tumor characterization using small subregions vs. whole tumor regions of interest. *PLoS One* 2015;10(10):e0138702.
15. El Khoulil RH, Jacobs MA, Mezban SD, et al. Diffusion-weighted imaging improves the diagnostic accuracy of conventional 3.0-T breast MR imaging. *Radiology* 2010;256(1):64–73.
16. Rahbar H, Zhang Z, Chenevert TL, et al. Utility of diffusion-weighted imaging to decrease unnecessary biopsies prompted by breast MRI: a trial of the ECOG-ACRIN Cancer Research Group (A6702). *Clin Cancer Res* 2019;25(6):1756–1765.
17. American College of Radiology Imaging Network (ACRIN) 6702 Protocol Documents. <https://www.acr.org/Research/Clinical-Research>. Accessed November 3, 2020.
18. American College of Radiology Imaging Network (ACRIN) 6702 Imaging Manual. <https://www.acr.org/Research/Clinical-Research>. Accessed November 3, 2020.
19. Morris EA, Comstock CE, Lee CH, et al. ACR BI-RADS magnetic resonance imaging. In: *ACR BI-RADS Atlas, Breast Imaging Reporting and Data System*. Reston, Va: American College of Radiology, 2013.
20. Rahbar H, Kurland BF, Olson ML, et al. Diffusion-weighted breast magnetic resonance imaging: a semiautomated voxel selection technique improves interreader reproducibility of apparent diffusion coefficient measurements. *J Comput Assist Tomogr* 2016;40(3):428–435.
21. Lee JM, Ichikawa L, Valencia E, et al. Performance benchmarks for screening breast MR imaging in community practice. *Radiology* 2017;285(1):44–52.
22. D’Orsi CJ, Sickles EA, Mendelson EB, Morris EA. *BI-RADS Atlas, Breast Imaging Reporting and Data System*. Reston, Va: American College of Radiology, 2013.
23. Rutter CM. Bootstrap estimation of diagnostic accuracy with patient-clustered data. *Acad Radiol* 2000;7(6):413–419.
24. LeDell E, Petersen M, van der Laan M. Computationally efficient confidence intervals for cross-validated area under the ROC curve estimates. *Electron J Stat* 2015;9(1):1583–1607.
25. Kuhl CK, Strobel K, Bieling H, Leutner C, Schild HH, Schrading S. Supplemental breast MR imaging screening of women with average risk of breast cancer. *Radiology* 2017;283(2):361–370.
26. Bakker MF, de Lange SV, Pijnappel RM, et al. Supplemental MRI screening for women with extremely dense breast tissue. *N Engl J Med* 2019;381(22):2091–2102.
27. Feig S. Cost-effectiveness of mammography, MRI, and ultrasonography for breast cancer screening. *Radiol Clin North Am* 2010;48(5):879–891.
28. Zhang L, Tang M, Min Z, Lu J, Lei X, Zhang X. Accuracy of combined dynamic contrast-enhanced magnetic resonance imaging and diffusion-weighted imaging for breast cancer detection: a meta-analysis. *Acta Radiol* 2016;57(6):651–660.
29. Chen X, Li WL, Zhang YL, Wu Q, Guo YM, Bai ZL. Meta-analysis of quantitative diffusion-weighted MR imaging in the differential diagnosis of breast lesions. *BMC Cancer* 2010;10(1):693.
30. Surov A, Meyer HJ, Wienke A. Can apparent diffusion coefficient (ADC) distinguish breast cancer from benign breast findings? A meta-analysis based on 13 847 lesions. *BMC Cancer* 2019;19(1):955.
31. Dorrius MD, Dijkstra H, Oudkerk M, Sijens PE. Effect of b value and pre-admission of contrast on diagnostic accuracy of 1.5-T breast DWI: a systematic review and meta-analysis. *Eur Radiol* 2014;24(11):2835–2847.
32. Pereira FP, Martins G, Figueiredo E, et al. Assessment of breast lesions with diffusion-weighted MRI: comparing the use of different b values. *AJR Am J Roentgenol* 2009;193(4):1030–1035.
33. Iima M, Kataoka M, Kanao S, et al. Intravoxel incoherent motion and quantitative non-Gaussian diffusion MR imaging: evaluation of the diagnostic and prognostic value of several markers of malignant and benign breast lesions. *Radiology* 2018;287(2):432–441.
34. Li T, Yu T, Li L, et al. Use of diffusion kurtosis imaging and quantitative dynamic contrast-enhanced MRI for the differentiation of breast tumors. *J Magn Reson Imaging* 2018;48(5):1358–1366.
35. Rydhög A, Pasternak O, Ståhlberg F, Ahlgren A, Knutsson L, Wirestam R. Estimation of diffusion, perfusion and fractional volumes using a multi-compartment relaxation-compensated intravoxel incoherent motion (IVIM) signal model. *Eur J Radiol Open* 2019;6:198–205.